DETC2003 / DAC-48730

TOPOLOGY OPTIMIZATION OF MULTI-COMPONENT STRUCTURES VIA DECOMPOSITION-BASED ASSEMBLY SYNTHESIS

Naesung Lyu and **Kazuhiro Saitou***
Department of Mechanical Engineering
University of Michigan
Ann Arbor, MI 48109-2125, USA
E-mail:{nlyu,kazu}@umich.edu

ABSTRACT

A method is presented for synthesizing multi-component structural assemblies with maximum structural performance and manufacturability. The problem is posed as a relaxation of decomposition-based assembly synthesis [1,2,3], where both topology and decomposition of a structure are regarded as variables over a ground structure with non-overlapping beams. A multi-objective genetic algorithm [4,5] with graph-based crossover [6,7,8], coupled with FEM analyses, is used to obtain Pareto optimal solutions to this problem, exhibiting trade-offs among structural stiffness, total weight, component manufacturability (size and simplicity), and the number of joints. Case studies with a cantilever and a simplified automotive floor frame are presented, and representative designs in the Pareto front are examined for the trade-offs among the multiple criteria.

INTRODUCTION

Most structural products have complex geometry to meet customer's demand of high functionality with enhanced structural stability. However, manufacturing those products in one piece requires sophisticated methods of process that will increase the total production cost. For this reason, most structural products are multi-component structures: they are made of number of components and these components are assembled into the final structure. Designing a multi-component structural product often requires designers to decompose overall product geometry at some point during the design process. The decomposition will determine the component set to be assembled into the final product.

For instance, automotive industry utilizes a handful of basic decomposition schemes of a vehicle taking into account of geometry, functionality, and manufacturing issues. However, those decomposition schemes are usually non-systematic and have remained more or less unchanged for decades. This is because the desired form, functionality, materials, joining methods and overall weight distribution of mass-production vehicles have not changed much for decades. However, the conventional decomposition schemes may no longer be valid for the vehicles with new technologies such as space frame, ultra-light weight materials, and fuel cell or battery powered motors, which would require dramatically different structural properties, weight distribution, and packaging requirements. This motivates the development of a systematic decomposition methodology presented in this paper.

In our previous work [1,2,3], we have termed *assembly synthesis* as the decision of which component set can achieve a desired function of the end product when assembled together, and assembly synthesis is achieved by the decomposition of product geometry. Since assembly process generally accounts for more than 50% of manufacturing costs and also affects the product quality [9], assembly synthesis would have a large impact on the quality and cost of the end product. In [3], we proposed a systematic method for decomposing a given product geometry considering the structural stiffness of the end product, where joints are modeled as torsional springs. During the work, it was observed that the structural integrity (*e.g.* stiffness) of the end-product is heavily influenced by the choice of a particular decomposition, as well as the given topology of the structure provided as an input of decomposition. This observation led us to a natural relaxation of the problem where

---

* corresponding author

both topology and decomposition of a structure are regarded as variable. This is the problem addressed in the present paper.

In this paper, topology and decomposition of a structure are simultaneously optimized over a ground structure with non-overlapping beams, for overall structural performance and manufacturability. As in [3], the joints between components are modeled as torsional springs. A multi-objective genetic algorithm with graph-based crossover, coupled with FEM analyses, is used to obtain Pareto optimal designs, exhibiting trade-offs among structural stiffness, total weight, component manufacturability (size and simplicity), and the number of joints. Case studies with a cantilever and a simplified automotive floor frame are presented, and representative designs in the Pareto front are examined for the trade-offs among the multiple criteria.

RELATED WORK

Structural topology optimization

Structural optimization can be classified into tree categories: topology optimization, shape optimization, and size optimization [10]. Among these tree categories, topology optimization is considered as the most general optimization problem with largest design space that can produce solutions with no prior assumptions. As one of the topology optimization methods, ground structure approach was first proposed by Dorn et al [11]. In the ground structure approach, optimal substructures can be found as a subset of predefined exhaustive set of discrete beam elements in an extended design domain (*i.e.*, ground structure). Extensive researches have been done to develop numerical methods for the topology design using ground structures: layout theory for frames and flexural systems [12,13], an approach using branch and bound algorithm [14], simulated annealing [15], and genetic algorithm [16]. More detailed development on the ground structure approach can be found in [17,18].

Another class of topology optimization method assumes structures made from solid continuum, rather than from discrete beams, where topology optimization problem is formulated as a material distribution problem within an extended design domain. Homogenization Design Method (HMD) is a representative of such "continuum-based" topology optimization methods [19], where material inside an extended design domain is treated as a composite material made of microstructures consisting of material and void. HMD has been applied to a broad range of problems including multiple loading problems [20], compliant mechanism design problems [21], multiple constraints problems [22], and topology optimization problems with composite material [23]. More closely related to the present work, several researchers investigated the homogenization-based topology optimization of multi-component structures [24,25,26,27]. These approaches, however, requires overlapping extended design domains for each component and each joint as a predefined input.

Design for assembly and assembly sequence design

Boothroyd and Dewhurst [28] are widely regarded as major contributors in the formalization of design for assembly (DFA) concept. In their work [29], assembly costs are first reduced by the reduction of part count, followed by the local design changes of the remaining parts to enhance their assembleability and manufacturability. This basic approach is adopted by most subsequent works on DFA. Many researchers have investigated the integration of DFA and assembly sequence planning [30, 31], where assembly sequence planning is proposed as the enumeration of geometrically feasible cut-sets of a liaison graph, an undirected graph representing the connectivity among components in an assembly. In order to improve the quality of the best assembly sequence, usually local design changes are made to the components These works, however, focus on the local design changes of a given assembly design (*i.e.*, already "decomposed" product design with "given" topology), and have less emphasis on *how to synthesize* an assembly to start with.

APPROACH

This section describes our method for synthesizing multi-component structural assemblies with maximum structural performance and manufacturability. Topology of a structure is represented as a subset of a ground structure consisting of an exhaustive set of non-overlapping beams (we call them *basic members*) within a given design domain. Joints within a structure are modeled as torsional springs, which can be placed only at the intersections of basic members in the ground structure. Joints are assumed to be less stiff than the beam elements and therefore reduce the overall structural rigidity.

Topology of a ground structure can be represented by *ground topology graph* $G_0 = (V_0, E_0)$ with node set V_0 of the basic members and edge set E_0 of the intersections of the basic members (*i.e.*, potential joint locations in the ground structure). Similarly, we represent the topology of a multi-component structural by *product topology graph* $G = (V, E, J)$, a subgraph of G_0 augmented with *joint set* $J \subseteq E$ specifying the location of joints. Using these notations, the following steps outline the approach:

1. Given a design domain with boundary and loading conditions (Figure 1 (a)), define the ground structure (Figure 1 (b)).
2. Construct the ground topology graph $G_0 = (V_0, E_0)$ for the ground structure (Figure 1 (c)).
3. Using an optimization algorithm (Figure 1 (d)), obtain the product topology graph $G = (V, E, J)$ that gives the best structural performance and manufacturability, (Figure 1 (e)).
4. Construct the multi-component structure corresponding to G (Figure 1 (f)).
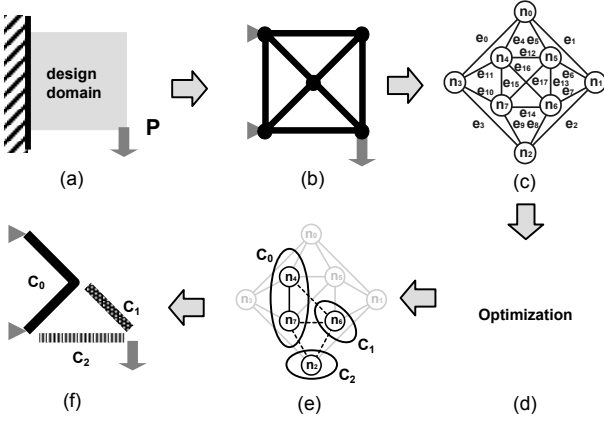
Figure 1. Outline of the approach. (a) Design domain, (b) ground structure consisting of basic members and potential joint locations, (c) ground topology graph G_0, (d) optimization, (e) best product topology graph G (subgraphs representing components are annotated as C_1-C_3, and edges in joint set J is shown in dashed lines), and (f) optimal multi-component structure.

Definition of design variables

In order to uniquely specify a product topology graph $G = (V, E, J)$, two binary vectors x and y are defined as design variables. *Topology vector* x represents the existence of each basic member (a node in ground topology graph G_0) in a multi-component structure represented by product topology graph G:

$$x = (x_0, x_1, \ldots, x_i, \ldots, x_{n-2}, x_{n-1}) \quad (1)$$

where $n = |V_0|$ and

$$x_i = \begin{cases} 1 & \text{if basic member } i \text{ exisits in the structure} \\ 0 & \text{otherwise} \end{cases}$$

For a given x, therefore, node set V of G can be written as:

$$V = \{n_i \in V_0 \mid x_i = 1\} \quad (2)$$

and edge set E as:

$$E = \{e \mid e = \{u, v\} \in E_0, u \in V, v \in V\} \quad (3)$$

In Figure 1 (e), for example, the gray nodes indicate the corresponding basic members with $x_i = 0$.

Decomposition vector y represents the *non*-existence of a joint (in other words, the existence of a solid connection) at each intersection of basic members (an edge in ground topology graph G_0) in a multi-component structure represented by product topology graph G:

$$y = (y_0, y_1, \ldots, y_i, \ldots, y_{m-2}, y_{m-1}) \quad (4)$$

where $m = |E_0|$ and

$$y_i = \begin{cases} 0 & \text{if a joint exisists in the structure at intersection } i \\ 1 & \text{otherwise} \end{cases}$$

Naturally, joint set J of G for a given y can be written as:

$$J = \{e_i \mid e_i \in E, y_i = 0\} \quad (5)$$

In Figure 1 (e), for example, the edges in dashed lines indicate joints, *i.e.*, the intersections with $y_i = 0$. The value of y_i is simply ignored if the corresponding intersection does not exist in the structure, *i.e.*, if edge $e_i \notin E$. In Figure 1 (e), the values of y_i are ignored for the intersections corresponding to the edges in gray lines.
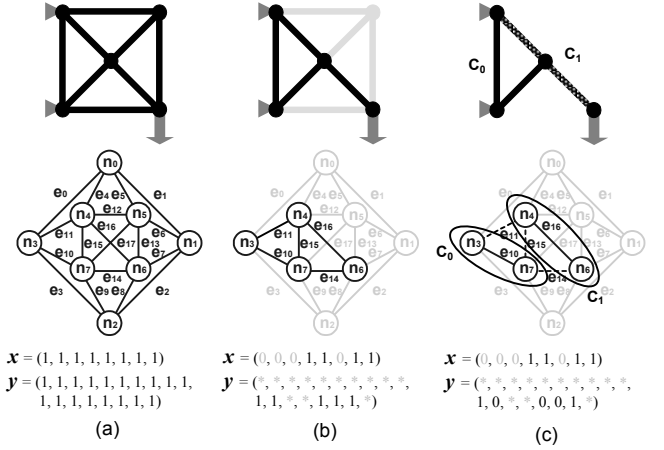
Figure 2. Multi-component structures represented by topology vector x and decomposition vector y.

Figure 2 illustrates examples of topology and decomposition represented by x and y. Figure 2 (a) shows a one-component structure identical to the ground structure with 8 nodes $V = \{n_0, n_1, \ldots, n_7\}$ and 18 edges $E = \{e_0, e_1, \ldots, e_{17}\}$. In this case, the corresponding topology vector is $x = (x_0, x_1, \ldots, x_7) = (1,1,1,1,1,1,1,1)$ and decomposition vector is $y = (y_0, y_1, \ldots, y_{17}) = (1,1,1,1,1,1,1,1,1,1,1,1,1,1,1,1,1,1)$. Figure 2 (b) illustrates a one-component structure represented by topology vector $x = (0,0,0,1,1,0,1,1)$, which can be obtained by removing basic members with $x_i = 0$ from the ground structure. Since this structure is made of one component, the topology vector should be of the form $y = (*, *, *, *, *, *, *, *, *, *, *, 1, 1,*, *,1,1,1,*)$, where symbol * means either zero or one, corresponding to the ignored edges shown in gray lines. Figure 2 (c) shows a decomposition of the structure in Figure 2 (b) into two components C_0 and C_1, represented by decomposition vector $y = (*,*, *, *, *, *, *, *, *, *, 1,0,*,*,0,0,1,*)$. Since y_{11}, y_{14} and y_{15} are 0, corresponding edges e_{11}, e_{14} and e_{15} are shown in

dotted lines, indicating the existence of joints (torsional springs) at the corresponding intersections.
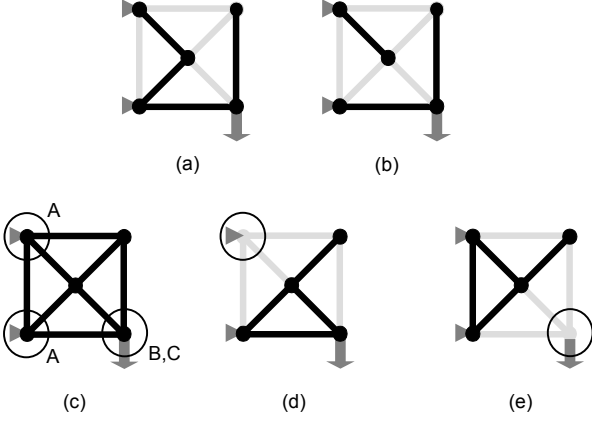
Figure 3. Constraints for feasible topology. (a) feasible structure, (b) infeasible structure violating Connectivity Constraint 1, (c) points considered in Connectivity Constraint 2. A: boundary condition, B: loading, and C: displacement, (d) infeasible topology violating Connectivity Constraint 2 (point A not connected), and (e) infeasible topology violating Connectivity Constraint 2 (point B-C not connected).

Definition of constraints

Topology of the structure defined by the topology vector x must satisfy the following constraints to avoid infeasible topologies as a mechanical structure:

- **Connectivity Constraint 1:** All beams should be connected to at least one other beam element, *i.e.*, product topology graph G should be connected (Figures 3 (a) and (b)).

- **Connectivity Constraint 2:** The following points should be connected to at least one beam element (Figures 3 (c), (d), and (e)):
  - points at which boundary conditions are defined;
  - points at which loads are applied;
  - points at which displacements are measured for the evaluation of structural performance.

Connectivity Constrains 1 can be formally written as:

$$\text{IS\_CONNECTED}(\text{GRAPH}(x, y_1)) = \text{TRUE} \qquad (6)$$

where x is a topology vector and y_1 is the decomposition vector with all components equal to one, $\text{GRAPH}(x, y)$ is a function that returns the product topology graph specified by x and y, and $\text{IS\_CONNECTED}(G)$ is a function that checks the connectivity of product topology graph G. Connectivity Constraint 2 can be written as:

$$\left(\prod_{i=1}^{N_{BP}} \sum_{j \in S_{BP_i}} x_j \right) \cdot \left(\prod_{i=1}^{N_{LP}} \sum_{j \in S_{LP_i}} x_j \right) \cdot \left(\prod_{i=1}^{N_{DP}} \sum_{j \in S_{DP_i}} x_j \right) \neq 0 \qquad (7)$$

where N_{BP}, N_{LP}, and N_{DP} are the number of points at which boundary conditions are defined, loads are applied, and displacements are measured, respectively. S_{BPi}, S_{LPi}, and S_{DPi} are sets of the indices of basic members attached to the ith point at which boundary conditions are defined, loads are applied, and displacements are measured, respectively.

Definition of objective functions

A multi-component structure represented by a topology vector x and a decomposition vector y is evaluated according to the following four criteria: 1) stiffness of the structure, 2) weight of the structure, 3) manufacturability of each component in the structure, and 4) numbers of joints (torsional springs) in the structure.

Stiffness of a structure can be measured as the negative of the displacement at predefined points in the structure:

$$f_{\text{stiffness}} = -\text{DISPLACEMENTS}(\text{GRAPH}(x, y)) \qquad (8)$$

where $\text{DISPLACEMENTS}(G)$ is a function that returns the total displacements at predefined points in the structure represented by product topology graph G, using finite element analyses.

Weight of a structure can be calculated as the inner product of topology vector x and vector w of the weights of the basic members in the ground structure:

$$f_{\text{weight}} = w \bullet x \qquad (9)$$

Manufacturability of components (to be maximized) is evaluated considering the total cost of producing components in the structure (to be minimized) represented by a product topology graph $\text{GRAPH}(x, y)$. It is assumed the components are made from sheet metals working, whose cost is estimated as the cost of stamping and blanking dies. The die costs consist of die set cost and die machining cost, which are functions of die usable area Au and shearing perimeter P, respectively [29]. For each component, Au is approximated as the convex hull area of given component and P is calculated as the outer perimeter of the component. Hence, larger size of the component results in higher value of Au requiring larger die set with higher cost. Also, complex geometry of component increases P value accompanied by higher die machining cost.

Following equation is used to calculate manufacturability of a structure:

$$f_{\text{manufac}} = W_{\text{au}}(1 - Au(\text{GRAPH}(x, y)) \\ + W_{\text{p}}(1 - P(\text{GRAPH}(x, y)) \qquad (10)$$

where $Au(G)$ and $P(G)$ calculate the normalized die usable area and normalized shearing perimeter of the components in the structure represented by G, respectively, and W_{au} and W_p are the weighting factors. Qualitatively, maximizing $f_{manufac}$ would result in a structure consisting of components in smaller sizes and in simpler geometries.

Components are assumed to be joined with spot welds. Since the cost of spot welding for a structure is proportional to the number of weld spots in the structure, and the number of weld spots in a joint is approximately proportional to the torsional stiffness of the joint, the welding cost is estimated by the sum of the rates of torsional springs [Nm/rad] in the finite element model of the structure:

$$f_{springrate} = \text{SPRINGRATE}(\text{GRAPH}(\boldsymbol{x}, \boldsymbol{y})) \qquad (11)$$

where TOTALSPRINGRATE(G) calculates the sum of the spring rates in FE model defined by graph G.

In summary, the multi-objective optimization problem to be solved can be stated as follows:

$$
\begin{aligned}
\text{maximize} \quad & f_{stiffness} = -\text{DISPLACEMENTS}(\text{GRAPH}(\boldsymbol{x}, \boldsymbol{y})) \\
\text{minimize} \quad & f_{weight} = \boldsymbol{w} \bullet \boldsymbol{x} \\
\text{maximize} \quad & f_{manufac} = W_{au}(1 - Au(\text{GRAPH}(\boldsymbol{x}, \boldsymbol{y})) \\
& \qquad\qquad + W_p(1 - P(\text{GRAPH}(\boldsymbol{x}, \boldsymbol{y})) \\
\text{minimize} \quad & f_{springrate} = \text{SPRINGRATE}(\text{GRAPH}(\boldsymbol{x}, \boldsymbol{y}))
\end{aligned}
$$

subject to
$$\text{IS\_CONNECTED}(\text{GRAPH}(\boldsymbol{x}, \boldsymbol{y}_1)) = \text{TRUE}$$

$$\left(\prod_{i=1}^{N_{BP}} \sum_{j \in S_{BP_i}} x_j \right) \cdot \left(\prod_{i=1}^{N_{LP}} \sum_{j \in S_{LP_i}} x_j \right) \cdot \left(\prod_{i=1}^{N_{DP}} \sum_{j \in S_{DP_i}} x_j \right) \neq 0$$

$$\boldsymbol{x} \in \{0,1\}^{|V_0|}, \boldsymbol{y} \in \{0,1\}^{|E_0|}$$

Optimization Algorithm

Due to the multi-objective formulation (as opposed to, *e.*g., weighted sum of multiple objectives) and the complexity of the underlying graph partitioning problem [32], the above optimization problem is solved using a multi-objective genetic algorithm (MOGA) [4,5], whose basic steps [5] are outlined below:

1. Create a population P of n chromosomes (an encoded representation of design variables) and evaluate their values of objective functions.
2. Rank each chromosome c in P according to the number of other chromosomes dominating c in Pareto sense (rank 0 is Pareto optimal). Store the chromosomes with rank 0 into set O. Also, create an empty subpopulation Q.
3. Select two chromosomes c_i and c_j in P with probability proportional to n-$rank(c_i)$ and n-$rank(c_j)$.
4. Crossover c_i and c_j to generate two new chromosomes c_i' and c_j' with a certain high probability.
5. Mutate c_i' and c_j' with a certain low probability.

6. Evaluate the objective function values of c_i' and c_j' and store them Q. If Q contains less than m new chromosomes, go to 3.
7. Let $P \leftarrow P \cup Q$ and empty Q, Rank each chromosome in P and remove m chromosomes with lowest ranks from P.
8. Update set O and increment the generation counter. If the generation counter has reached a pre-specified number, terminate the process and return O. Otherwise go to 3.

Since two design variables, topology vector $\boldsymbol{x}$ and decomposition vector $\boldsymbol{y}$, are binary vectors, the components of $\boldsymbol{x}$ and $\boldsymbol{y}$ are simply laid out in a linear chromosome of length $|V|+|E|$ as illustrated in Figure 4.
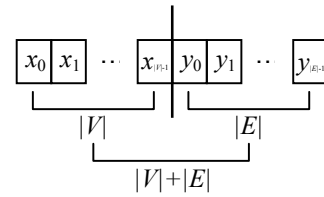
Figure 4. Chromosome representation of design variables x and y, where the elements of these vectors are simply laid out to form a linear chromosome of length $|V|+|E|$.

Crossover in step 4 combines "genetic materials" of two parent chromosomes to produce two offspring chromosomes. The role of crossover is to combine high-quality partial solutions (building blocks) in parent chromosomes to produce higher quality offspring [33]. Since information in $\boldsymbol{x}$ and $\boldsymbol{y}$ are linked in a non-linear fashion as defined in the ground topology graph, the conventional one point or multiple point crossover for linear chromosomes will not effectively preserve the building blocks. For this type of problem, *graph-based crossover* has been successfully applied for improved performance of GA [6,7,8], which is adapted to fit to our problem as described below:

1. Draw an arbitrary crossover line L on two parent structures $P1$ and $P2$, and use the line to "cut" $P1$ into two substructures $S11$ and $S12$, and $P2$ into $S2$ and $S22$ (Figure 5 (a)).
2. Partition product topology graphs of $P1$ to two subgraphs $G11$ and $G12$ corresponding to $S11$ and $S12$. Do the similar to partition the graph of $P2$ to $G21$ and $G22$ (Figure 5 (b)).
3. Assemble an offspring graph with $G11$ and $G22$, and another with $G21$ and $G12$. During the assembly process, edges between two nodes came from different parents are randomly assigned (Figure 5 (c)).
4. Construct offspring structures using the assembled graphs (Figure 5 (d)).
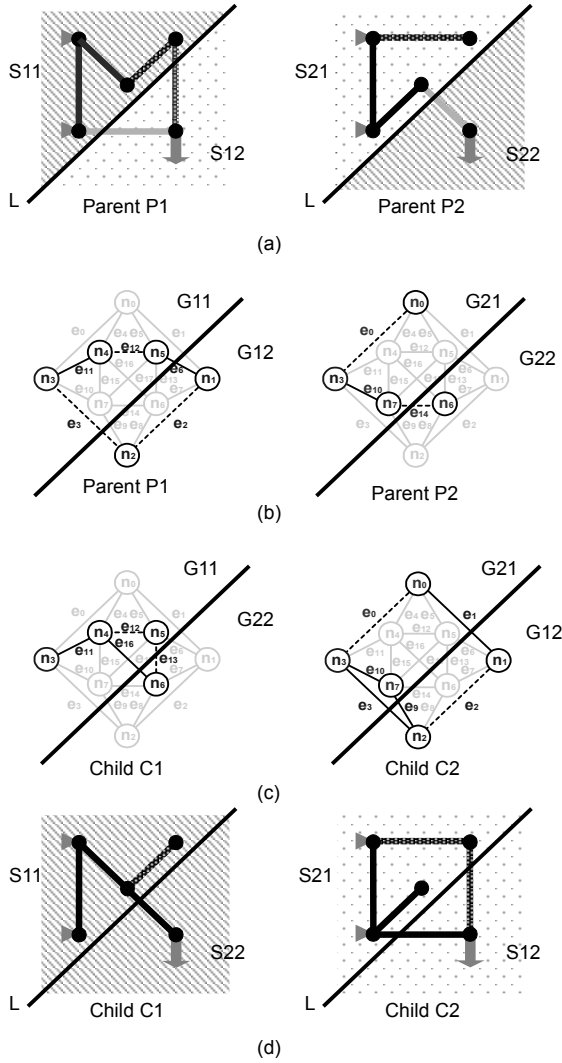
Figure 5. Graph-based crossover operation. (a) Parent structures *P1* and *P2* cut by crossover line *L*, (b) corresponding partitioning of *P1* and *P2* in graph representation, (c) assembly of offspring graphs *C1* and *C2*. Note that in *C1*, edges e_{11} and e_{12} are copied from parent *P1* because nodes n_3, n_4, and n_5 are from *P1*. Edges e_{16} and e_{13} are randomly assigned because n_6 is form *P2* while n_4 and n_5 are from *P1*. (d) Offspring structures *C1* and *C2* constructed from their graphs. Both *C1* and *C2* have 2 components.

Crossover line *L* is selected in the geometrical space (where the physical structures belong) rather than in the topological space (where the product topology graphs belong) to realize the effective preservation of smaller high-quality substructures – building blocks for our problem.

Even though both parent graphs are connected, the crossover may yield an offspring graphs *C* that are disconnected. In such cases, a repair operator is applied to reconstruct the connectivity, where Dijkstra's algorithm [34] is used to find the shortest path on the ground topology graph between the disconnected subgraphs of *C*, and the nodes and edges on the shorted path are added to *C*.

Mutation modifies a structure in the following three steps:

1. Mutate topology vector *x* by random bit flipping. This will add or remove basic members (Figures 6 (b) and (c)).
2. If the resulting structure is disconnected, apply the above repair operator to reconstruct connectivity.
3. Mutate decomposition vector *y* by random bit flipping. This will alter the location of joints (Figure 6 (d)).
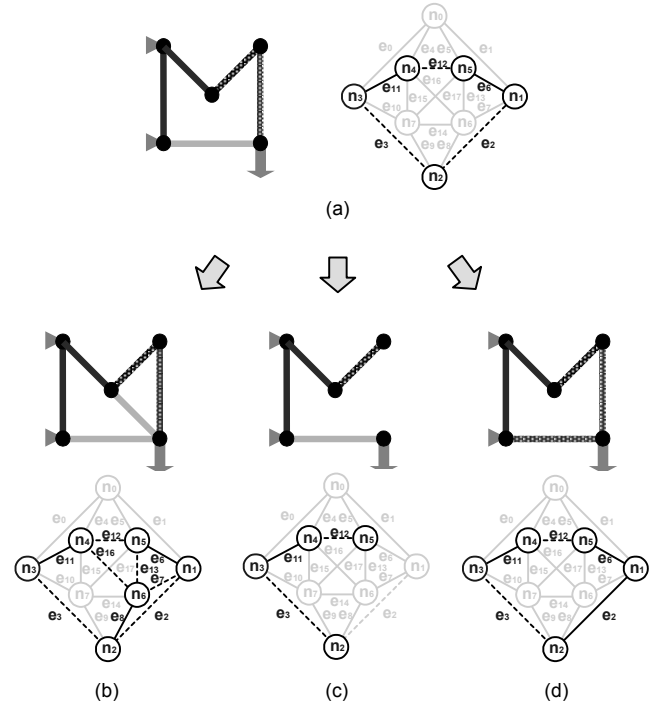
Figure 6. Mutation operation. (a) original structure and graph (b) adding beam elements, (c) removing beam elements, and (d) altering joint locations.

In addition to the above custom crossover and mutation, the implementation of MOGA used in the following examples utilizes linear fitness scaling, niching based on the distances in objective function space, and stochastic universal sampling [5]. Also, the population is initialized to contain only chromosomes that satisfy both Connectivity Constraints 1 and 2. Figure 7 shows the flowchart of multi-component structure synthesis. Software implementation, including MOGA code, is done in the C++ programming language. LEDA[1] library was used for graph algorithm and an in-house FEM code[2] is used to obtain $f_{\text{stiffness}}$.

---

[1] Developed by Algorithmic Solution (http://www.algorithmic-solutions.com)
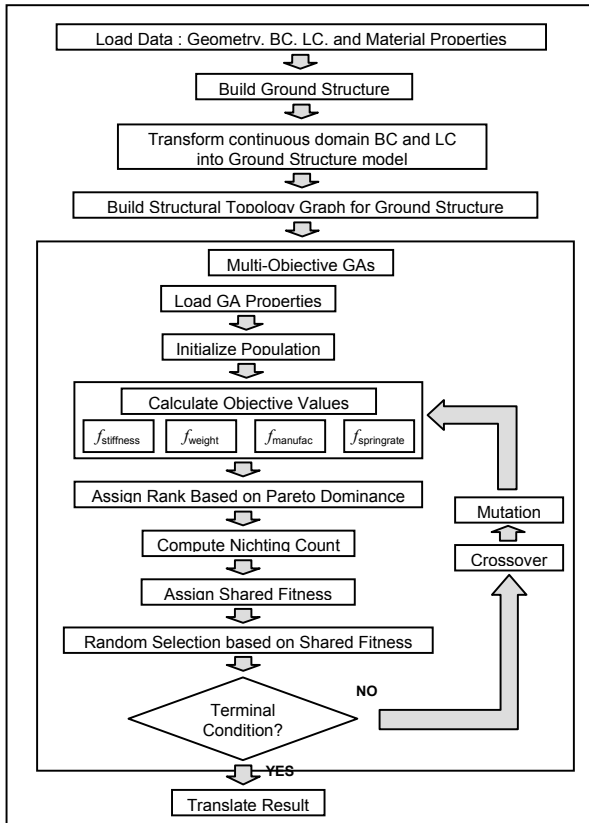[2] Developed by Mr. Karim Hamza.

Copyright © 2003 by ASME

Figure 7. Flowchart of multi-component structure synthesis.

CASE STUDY

Multi-component structure synthesis in Figure 7 is applied to two case studies: a cantilever structure and a simplified automotive floor frame. Tables 1 and 2 list the geometric and material properties of the beam elements and the parameter values for MOGA runs used in both case studies, respectively. The spring rate of 100,000[Nm/rad] is used for all torsional springs.

Table 1. Geometric and material properties of beam elements used in the case studies.

property	value
cross sectional area	314 [mm^2]
moment of inertia (I_{xx}, I_{yy})	7,854 [mm^4]
polar moment of inertia	15,708 [mm^4]
density	3194.0 [kg/m^3]
Young's modulus	210 [GPa]

Table 2. Parameter values for MOGA runs used in the case studies.

property	Case I
maximum # of generation	100
number of population	1000
replacement rate (m/n)	0.5
crossover probability	0.9
mutation probability for x	0.05 (case I)
	0.10 (case 2)
mutation probability for y	0.10

Case I: Cantilever Structure

For the first case study, a cantilever structure is modeled as a design domain in Figure 8 (a), with length 200 [mm] and height 100 [mm]. The left side of the domain is fixed on the wall and a vertical load P (=100 [N]) is applied at the lower right corner of the domain. The displacement is measured at the loading point to calculate the stiffness of the structure. Figure 8 (b) shows the ground structure with 15 non-overlapping beam elements, each of which are regarded as a basic member. Figure 8 (c) shows the ground topology graph of the ground structure in Figure 8 (b), containing 15 nodes and 44 edges.
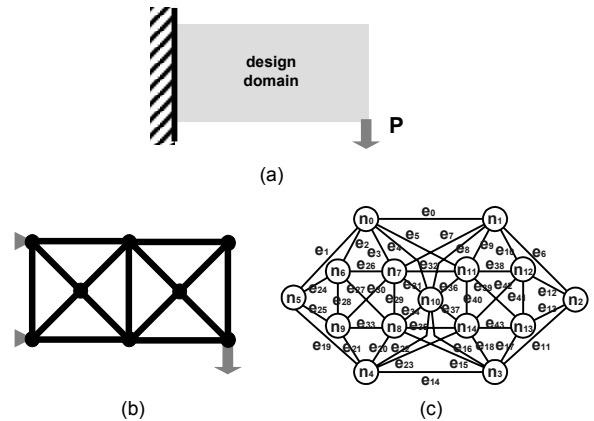

(a)

(b)   (c)

Figure 8. Case I model. (a) design domain, (b) ground structure with 15 beam elements, and (c) ground topology graph of 15 nodes (n_0~n_{14}) and 44 edges (e_0~e_{43}).

Figure 9 shows the typical convergence histories of MOGA runs with three different mutation probabilities for y (Figure 10 (a)). All three plots indicate the increase in the size of Pareto set (number of Pareto optimal designs) as the number of generation increases. Note that as mutation probability decreases, the number of individuals in the Pareto Front converges closer to the total number of population (= 1000).
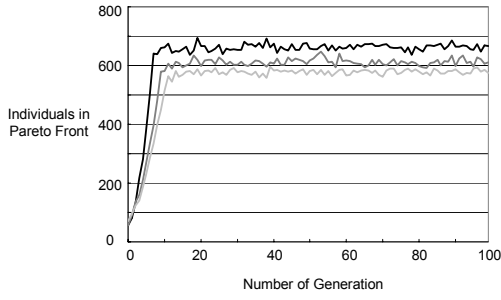
Figure 9. Typical convergence histories of MOGA runs with three different mutation probability for y (black line: 0.1, dark gray line: 0.2 and light gray line: 0.3).

Figure 10 shows objective function spaces obtained at the terminal generation (= 100). Because there are four objective functions, $f_{stiffness}$, f_{weight}, $f_{manufac}$, and $f_{springrate}$, the resulting 4-dimensional space is projected on to four 2-dimensional spaces as shown in Figures 10 (a)-(d). Each 2-D plot shows points for all 1000 structural designs with respect to the chosen two objectives only, ignoring the values of the remaining two objectives. In all plots, the utopia points are located at the upper right corner. The points with rank < 3 (with respect to all four objectives) are marked black in each plot. The following observations can be made from these plots:

- **Observation 1**: In $f_{weight} - f_{stiffness}$ space (Figure 10 (a)), designs are concentrated on the upper-right portion.
  Possible explanation: Higher weight implies more beams, which tends to increase stiffness.

- **Observation 2**: $f_{weight} - f_{manufac}$ space (Figure 10 (b)) shows a linear trend between f_{weight} and $f_{manufac}$.
  Possible explanation: Shearing perimeter (P) that determines $f_{manufac}$ is highly related to the f_{weight} because we are using only beam elements, where component perimeter is directly proportional to the size (and weight) of the element. As a result, higher manufacturability implies less number of beams, which decreases total weight.

- **Observation 3**: Designs with lower stiffness show higher manufacturability (Figure 10 (c)).
  Possible explanation: Higher manufacturability implies smaller components, which would require more joints, which in turn tends to reduce stiffness.

- **Observation 4**: Design with higher $f_{springrate}$ show lower stiffness (Figure 10 (d), upper portion).
  Possible explanation Higher $f_{springrate}$ implies more number of springs in the joints, which tends to reduce stiffness.


(a)　　　　　　　　　　(b)

(c)　　　　　　　　　　(d)
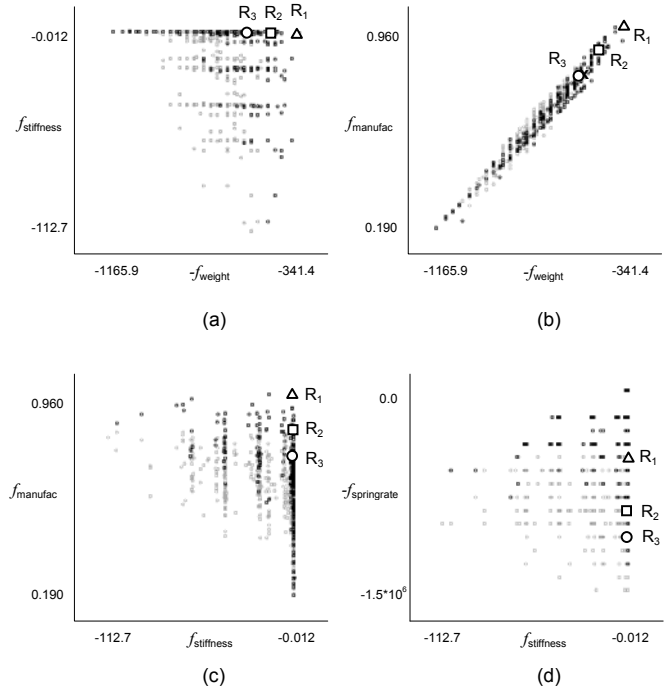
Figure 10. Distribution of designs at generation = 100 for Case I. In all plots, the utopia points are at the upper right corner. Black-marked ones are designs with rank<3 with respect to *all* four objectives. Three representative Pareto optimal designs R_1, R_2 and R_3 are shown in Figure 11.

Three representative Pareto optimal designs, annotated as R_1, R_2 and R_3 in Figure 10, are shown in Figure 11 and their objective function values are listed in the Table 3. Objective function values in Table 3 are plotted on a spider diagram in Figure 12. The geometry of each structure exhibits its unique characteristics allowing the following interpretations:

- Structure R_1 (Figure 11 (a)) is a very light structure with three simple components connected by 2 joints. Each joint design is composed of 2 torsional springs with spring rate 100[Nm/rad]. The structure also fairly stiff thanks to the clever arrangement of beams (including a triangular structure formed with the wall), which imposes mostly axial loading in each beam, thereby avoiding bending of joints.

- Structure R_2 (Figure 11 (b)) shows balanced performances in all objectives with very good stiffness. One component with the complex geometry (hence causing reduced manufacturability) seems the key to very high stiffness with low weight.

- Structure R_3 (Figure 11 (c)) has three components that are more complex and larger than the ones of R_1 and R_2. It is the stiffest among the three structures. It contains the

8　　　　　　　　　Copyright © 2003 by ASME

three triangular structures (including the one formed with the wall), which seems to help for increasing the stiffness of the structure.


(a)

(b)

(c)
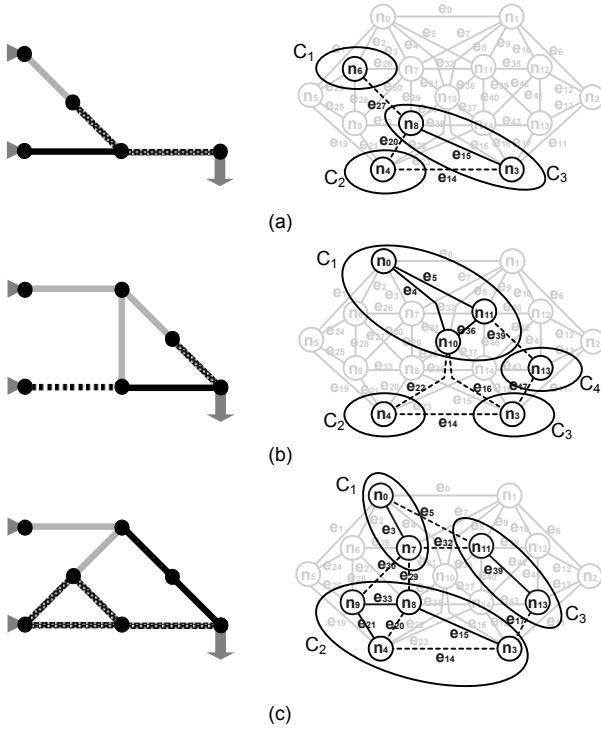
Figure 11. Representative Pareto optimal designs for Case I. (a) R_1, (b) R_2, and (c) R_3. R_1 and R_3 have 3 components and R_2 has 4 components.

Table 3. Objective function values for R_1, R_2, and R_3.

	$f_{stiffness}$ [mm]	f_{weight} [10^{-3}Kg]	$f_{manufac}$	$f_{springrate}$ [Nm/rad]
R_1	0.510	341.4	0.960	$0.4*10^6$
R_2	0.071	541.4	0.764	$0.7*10^6$
R_3	0.017	653.5	0.673	$0.8*10^6$

Case II: Simplified Automotive Floor Frame under Multiple Loadings

For the second case study, a simplified automotive floor frame under multiple loadings is modeled as a design domain in Figures 13 (a)-(c), with length 3000 [mm] and width 1600 [mm] seen from the above. The structure is subject to the following three loading cases:
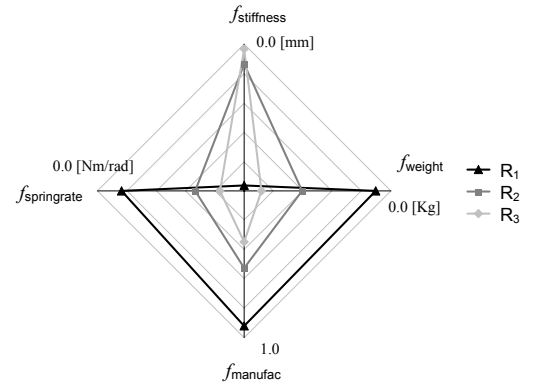

Figure 12. A spider diagram for the objective function values of designs R_1, R_2, and R_3. Note that R2 shows a balanced performance in all 4 objective functions.

1. Front wheel locations are fixed on the ground and a unit horizontal load $P_1 (= 1.0$ [N]) is applied at each of the right end points of the domain that represent rear wheel locations (Figure 13 (a)).
2. Rear wheel locations are fixed on the ground and a unit horizontal load $P_2 (= 1.0$ [N]) is applied at each of the left end points of the domain that represent front wheel locations (Figure 13 (b)).
3. Both of the front and rear wheel locations are fixed and unit horizontal load $P_3 (= 1.0$ [N]) is applied at the middle of the domain (Figure 13 (c)).

Displacements are measured at the loading points to calculate the stiffness of the structure. Since there are three values of displacements corresponding to the three loading cases, the number of objective functions becomes 6 (3 stiffness, 1 weight, 1 manufacturability, and 1 spring rates).

Figure 13 (d) illustrates the ground structure with 70 non-overlapping beam elements, each of which are regarded as a basic member. Due to the symmetric nature of the automotive floor frame, only right half of the floor frame will be modeled and the left side of the floor frame will have the mirror image of the right side. Figure 13 (e) shows the ground topology graph of upper half of the ground structure in Figure 13 (d), containing 38 nodes and 130 edges.

(a) (b) (c)

(d)

(e)
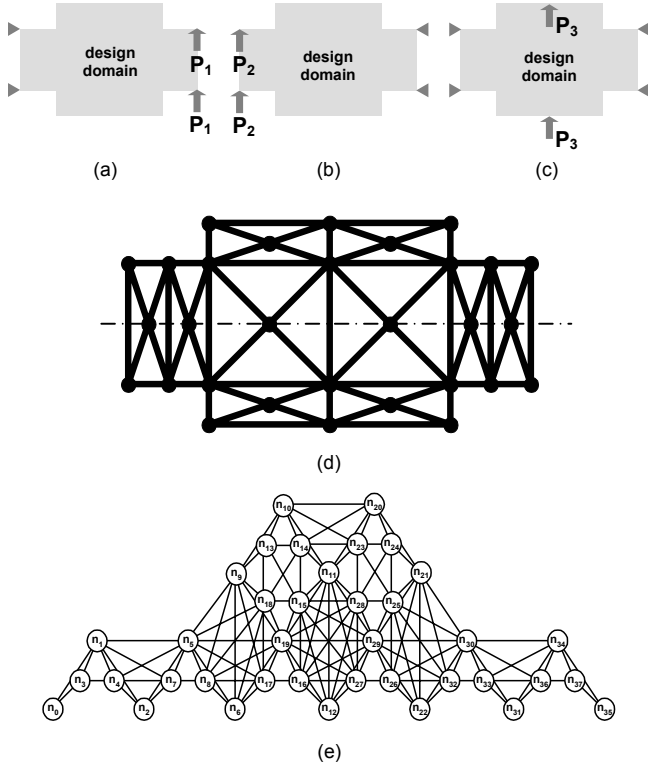
Figure 13. Case study II model. (a)~(c) Design domain with three loading and boundary conditions, (d) ground structure with 70 beam elements, and (e) ground topology for upper half model with 38 nodes (n_0~n_{37}) and 130 edges. Note that symmetric design assumption made only the beams in the upper half modeled in (e). Edge numbers (e_0~e_{129}) are not shown in (e) due to the space limitation.
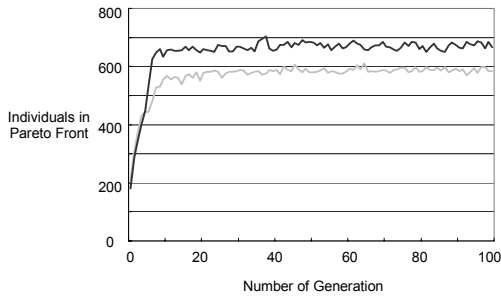
Figure 14. Typical convergence histories of MOGA runs with three different mutation probability for x (black line: 0.05, and gray line: 0.1).

Figure 14 shows the typical convergence histories of MOGA runs with two different mutation probabilities for x in Case II. As in Case I, all plots indicate the increase in the size of Pareto set (number of Pareto optimal designs) as the number of generation increases.

The six selected objective function spaces obtained at the terminal generation (= 100) are illustrated in Figure 15. Because there are six objective functions ($f_{stiffness\_1}$, $f_{stiffness\_2}$, $f_{stiffness\_3}$, f_{weight}, $f_{manufac}$, and $f_{springrate}$), the resulting 6-dimensional space is projected on to 2-dimensional spaces as shown in Figures 15 (a)-(f) as in Case I. The following observations can be made from these plots:

(a) (b)

(c) (d)

(e) (f)
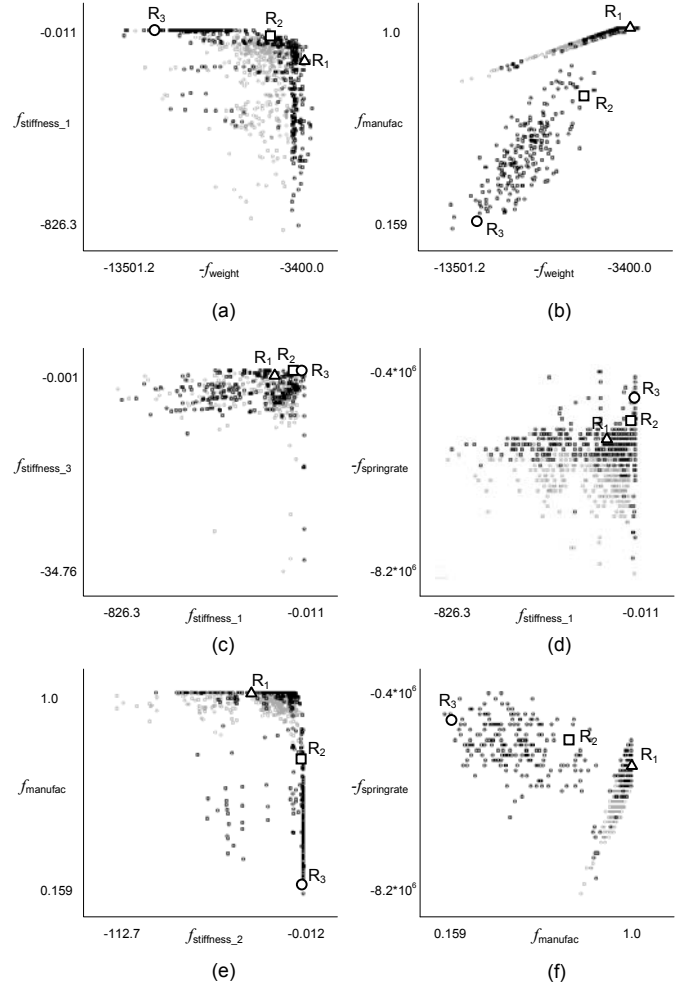
Figure 15. Distribution of designs at generation = 100. In all plots, the utopia points are at the upper right corner. Black-marked ones are designs with rank < 3 with respect to *all* six objectives. Three representative Pareto optimal designs R_1, R_2, and R_3 are shown in Figure 16.

- **Observation 1**: As in Case I, designs are concentrated on the upper-right portion in $f_{weight} - f_{stiffness\_1}$ space (Figure 15 (a)).
  Possible explanation: Higher weight implies more beams, which tends to increase stiffness.

- **Observation 2**: $f_{weight} - f_{manufac}$ space (Figure 15 (b)) shows two groups of solutions. While upper group is composed

Copyright © 2003 by ASME

of solutions mostly with beam-shaped components, lower group solutions contain more number of components with larger area. In the upper group, the strong linear trends can be seen between f_{weight} and $f_{manufac}$ as in Case I.

Possible explanation: As in Case I, in the structures composed of linear shaped components, higher manufacturability implies less number of beams, which decreases total weight.

- **Observation 3**: As in Case I, designs with higher $f_{springrate}$ show lower stiffness (Figure 15 (d), upper portion).
  Possible explanation: Higher $f_{springrate}$ implies more number of springs in the joints, which reduce stiffness.

- **Observation 4**: Designs with higher manufacturability show higher value of $f_{springrate}$ (Figure 15 (f)).
  Possible explanation: Higher manufacturability implies smaller components, which would require more joints, which in turn needs more springs.

(a)

(b)

(c)
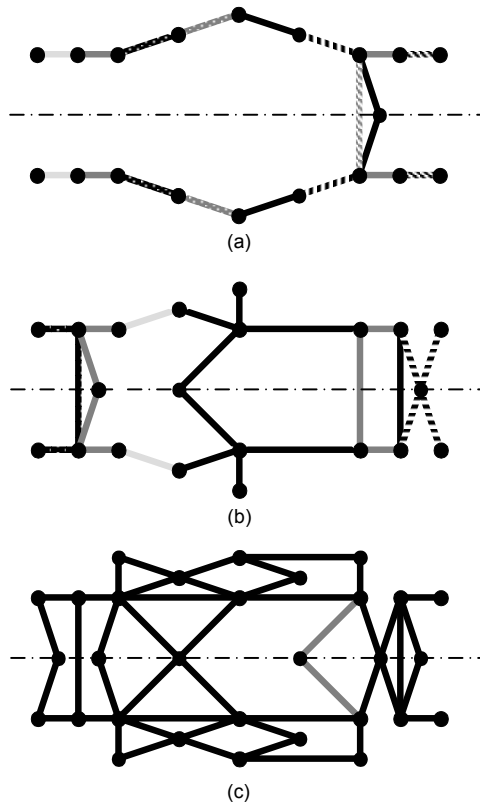
Figure 16. Representative Pareto optimal designs. (a) R_1, (b) R_2, and (e) R_3. R_1, R_2 and R_3 have 18, 8 and 2 components, respectively.
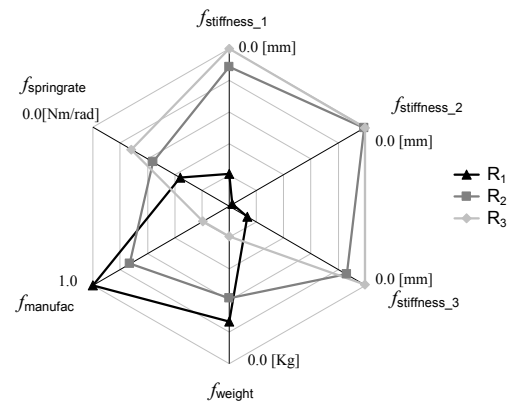
Three representative Pareto optimal designs, annotated as R_1, R_2 and R_3 in Figure 15, are shown in Figure 16 and their objective function values are listed in the Table 4. Objective

function values in Table 4 are plotted on a spider diagram in Figure 17. The geometry of each structure exhibits its unique characteristics allowing the following interpretations:

- Structure R_1 (Figure 16 (a)) is a light structure with 18 simple beam shape components connected by 14 joints. The structure shows high manufacturability due to the simple shapes of components with large number of joints sacrificing the stiffness characteristics. In Figure 17, Structure R_1 shows a biased performance on the f_{weight} and $f_{manufac}$.

- In Structure R_2 (Figure 16 (b)), one middle component with the complex geometry (hence causing reduced manufacturability) and closed box sub-structures in the middle of the structure seem to increase the stiffness of the structure with relatively low total weight. In Figure 17, Structure R_2 shows a well balanced performance on every objective functions.

- Structure R_3 (Figure 16 (c)) is the heaviest structure among these three structures and contains one big component that are more complex and larger than the ones of R_1 and R_2. Due to this complex component, manufacturability of this structure is low. However, it increased the stiffness of the structure in all three loading cases. In Figure 17, Structure R_3 shows a biased performance on the stiffness functions.

Table 4. Objective function values for $R_1 \sim R_3$ in Case II

	$f_{stiffness\_1}$ [mm]	$f_{stiffness\_2}$ [mm]	$f_{stiffness\_3}$ [mm]	f_{weight} [Kg]	$f_{manufac}$	$f_{springrate}$ [Nm/rad]
R_1	119.41	243.56	0.432	4.00	0.998	$3.2*10^6$
R_2	17.38	1.99	0.068	6.28	0.718	$2.2*10^6$
R_3	0.08	1.02	0.002	12.10	0.190	$1.4*10^6$

Figure 17. A spider diagram for the objective function values of the representative Pareto optimal designs ($R_1 \sim R_3$) in Case II. Note that R_2 shows a balanced performance in all 6 objective functions.

SUMMARY AND FUTURE WORK

This paper described a method for synthesizing multi-component structural assemblies, where the topology and decomposition of a structure is simultaneously optimized over a ground structure for stiffness, weight, component manufacturability, and assembleability. Multi-objective genetic algorithm, coupled with finite element analyses, was employed to efficiently obtain Pareto optimal designs for the four objectives. Two simple case studies were presented to demonstrate the effectiveness of the proposed method.

While the obtained results are inspiring, further relaxation of the optimization problem is desired, for example, by allowing variable spring rate at joints and variable cross section of beam elements. We also believe it would be possible to extend the present approach to continuum based topology optimization by extending the framework of, for example, the Homogenization Design Method [19]. The developments in these directions are currently in progress and will be reported at other future opportunities.

REFERENCES

[1] Yetis, A. and Saitou, K., 2002, "Decomposition-Based Assembly Synthesis Based on Structural Considerations," *ASME Journal of Mechanical Design*, v. 124, pp. 593–601.

[2] Cetin, O.L. and Saitou, K., 2001. "Decomposition-based assembly synthesis for maximum structural strength and modularity," *Proceedings of the 2001 ASME Design Engineering Technical Conferences*, September 9-12, 2001, Pittsburgh, PA, DETC2001/DAC-21121. An extended version accepted to *ASME Journal of Mechanical Design.*

[3] Lyu, N. and Saitou, K., 2002. "Decomposition-based assembly synthesis based on structural stiffness considerations", *Proceedings of the 2002 ASME Design Engineering Technical Conferences*, September 29 - October 2, 2002, Montreal, Canada, DETC2002/DAC-34083. An extended version accepted to *ASME Journal of Mechanical Design.*

[4] Fonseca, C. M. and Fleming, P. J., 1993. "Genetic Algorithms for Multiobjective Optimization: Formulation, Discussion and Generalization", *Proceedings of the Fifth International Conference on Genetic Algorithms*, San Mateo, California, pp. 416-423.

[5] Coello , C. A., Veldhuizen, D. A. and Lamont, G. B., 2002. *Evolutionary algorithms for solving multi-objective problems,* Kluwer Academic/Plenum Publishers, New York. pp. 72.

[6] Saab, Y. and Rao. V., 1990. "Stochastic evolution: A fast effective heuristic for some genetic layout problems", *27th ACM/IEEE Design Automation Conference*, pp. 26-31.

[7] Laszewski, G., 1991. "Intelligent structural operators for the k-way graph partitioning problem", *Fourth International Conference on Genetic Algorithms*, pp. 45-52.

[8] Pereira, F., Machado, P., Costa, E., and Cardoso, A., 1999. "Graph Based Crossover – A Case Study with the Busy Beaver Problem", *Proceedings of the 1999 Genetic and Evolutionary Computation Conference.*

[9] Lotter, B., 1989. *Manufacturing Assembly Handbook*, Butterworths, London.

[10] Howell, 2001. *Compliant Mechanisms*, John Wiley & Sons, New York. pp. 312.

[11] Dorn, W. C., Gomory, R.E., and Greenberg, H.J., 1964. "Automatic design of optimal structures", *J. Mec*. 3, 1964.

[12] Rozvany, G.. I., 1976. *Optimal Design of flexural systems*, Oxford: Pergamon

[13] Rozvany, G. I., 1992. *Shape and lay-out optimization in structural design*, CISM Lecture Notes No. 325. Vienna: Springer.

[14] Ringertz, U. T., 1986. A branch and bound algorithm for topology optimization of truss structure, *Eng Opt* 10, pp.111-124.

[15] Fleury, C., 1993. Discrete valued optimal design problems. In Bendsøe, M. P. and Mota Soares, C.A. (eds.) *Topology optimization of structure*, pp. 81-96. Dordrecht: Kluwer.

[16] Hajela, P., Lee, E., Lin, C. Y., 1993. Genetic algorithms in structural topology optimization. In Bendsøe, M. P. and Mota Soares, C.A. (eds.) *Topology optimization of structure*, pp. 117-134. Dordrecht: Kluwer.

[17] Kirsch, U., 1989. "Optimal topologies of structures", *Applied Mechanics Review,* Vol. 42, Aug 1989, pp. 223-249.

[18] Bendsøe, M. P., 1994. "Optimization methods for truss geometry and topology design", *Structural Optimization* 7, 1994, pp. 141-159.

[19] Bendsøe, M. P. and N. Kikuchi, 1988. "Generating optimal topologies in structural design using a homogenization method," *Computer Methods in Applied Mechanics and Engineering*, Vol. 71, pp. 197-224.

[20] Diaz, A. R. and Bendsøe, M. P., 1992. "Shape optimization of structures for multiple loading conditions using a homogenization method", *Structural Optimization*, 1992.

[21] Ananthasuresh, G.K., Kota, S., and Kikuchi, N., 1994. "Strategies for Systematic synthesis of Compliant MEMS", DSC-Vol. 55-2, *1994 ASME Winter Annual Meeting*, pp. 677-686.

[22] Jiang T., and Papalambros, P. Y., 1996. "Optimal structural topology design using homogenization method with multiple constraints", *Engineering Optimization,* 1996.

[23] Rodrigues, H, Guedes, J. M. and Bendsøe, M. P., 2002. "Hierarchical optimization of material and structure", *Structural and Multidisciplinary Optimization* Vol. 24, 2002, pp. 1-10.

[24] Chickermane, H. and Gea, H. C., 1997. "Design of Multi-Component Structural System for Optimal Layout Topology and Joint Locations", *Engineering with Computers* 13, 1997, pp. 235-243.

[25] Johanson, R., Kikuchi, N., and Papalambros, P., 1994. "Simultaneous Topology and Material Microstructure Design," *Advances in Structural Optimization*, B.H.V. Topping and M. Papadrakakis (ed.), Civil-Comp Ltd., Edinburgh, Scotland, pp. 143-149.

[26] Jiang, T. and Chirehdast, M., 1997. "A Systems Approach to Structural Topology Optimization: Designing Optimal Connections," *ASME Journal of Mechanical Design*, Vol. 119, pp. 40-47.

[27] Li, Q., Steven, G.P. and Xie, Y.M., 2001. "Evolutionary structural optimization for connection topology design of multi-component systems", *Engineering Computations*, Vol. 18 No. 3/4, 2001, pp. 460-479.

[28] Boothroyd, G. and Dewhurst, P., 1983. *Design for Assembly Handbook*, University of Massachusetts, Amherst.

[29] Boothroyd, G., Dewhurst, P., and Knight, W., 1994. *Product Design for Manufacturing and Assembly*, Marcel Dekker, New York.

[30] De Fanzio, T., and Whitney, D., 1987. "Simplified generation of all mechanical assembly sequences," *Transaction of IEEE, Journal of Robotics and Automation,* pp.640-658.

[31] Ko, H. and Lee, K., 1987. "Automatic assembling procedure generation from mating conditions," *Computer Aided Design* 1987, Vol. 19, pp. 3-10.

[32] Garey, M. R. and Johnson, D. S., 1979. *Computers And Intractability, a Guide to the Theory of NP-completeness*, W. H. Freeman and Company, New York.

[33] Goldberg, D., 1989. *Genetic Algorithms in Search, Optimization, and Machine Learning*, Addison-Wesley, Massachusetts.

[34] Dijkstra, E. W., 1959. "A note on two problems in connection with graph", *Num. Math.*, 1: pp. 269-271.